From surface to volume plasmons in hyperbolic metamaterials: General existence conditions for bulk high-k waves in metal-dielectric and graphene-dielectric multilayers.

Zhukovsky, Sergei; Andryieuski, Andrei; Sipe, John E.; Lavrinenko, Andrei

Published in:
Physical Review B Condensed Matter

Link to article, DOI:
10.1103/PhysRevB.90.155429

Publication date:
2014

Document Version
Publisher's PDF, also known as Version of record

From surface to volume plasmons in hyperbolic metamaterials: General existence conditions for bulk high-*k* waves in metal-dielectric and graphene-dielectric multilayers

Sergei V. Zhukovsky,[1,*] Andrei Andryieuski,[1] J. E. Sipe,[2] and Andrei V. Lavrinenko[1]
[1]*DTU Fotonik, Department of Photonics Engineering, Technical University of Denmark, Ørsteds Plads 343, DK-2800 Kongens Lyngby, Denmark*
[2]*Department of Physics and Institute for Optical Sciences, University of Toronto, 60 St. George Street, Toronto, Ontario, Canada M5S 1A7*
(Received 27 March 2014; revised manuscript received 15 September 2014; published 16 October 2014)

We theoretically investigate general existence conditions for broadband bulk large-wave-vector (high-*k*) propagating waves (such as volume plasmon polaritons in hyperbolic metamaterials) in subwavelength periodic multilayer structures. Describing the elementary excitation in the unit cell of the structure by a generalized resonance pole of a reflection coefficient and using Bloch's theorem, we derive analytical expressions for the band of large-wave-vector propagating solutions. We apply our formalism to determine the high-*k* band existence in two important cases: the well-known metal-dielectric and recently introduced graphene-dielectric stacks. We confirm that short-range surface plasmons in thin metal layers can give rise to hyperbolic metamaterial properties and demonstrate that long-range surface plasmons cannot. We also show that graphene-dielectric multilayers tend to support high-*k* waves and explore the range of parameteres for which this is possible, confirming the prospects of using graphene for materials with hyperbolic dispersion. The approach is applicable to a large variety of structures, such as continuous or structured microwave, terahertz, and optical metamaterials.

DOI: 10.1103/PhysRevB.90.155429 PACS number(s): 78.67.Pt, 41.20.Jb, 78.20.Ci, 42.70.−a

I. INTRODUCTION

Hyperbolic metamaterials (HMMs) are composite media that consist of subwavelength structures assembled so that an extreme anisotropy results on the macroscopic scale, with metallic behavior arising for one polarization of light and dielectric behavior for the other. In other words, in the idealization where a homogenization model is valid and an effective permittivity tensor can be introduced, this tensor $\varepsilon = \mathrm{diag}(\varepsilon_x,\varepsilon_y,\varepsilon_z)$ has eigenvalues of different signs, e.g., $\varepsilon_x = \varepsilon_y < 0$ and $\varepsilon_z > 0$ in the case of uniaxial anisotropy. We assume the choice of the coordinate system in which the tensor ε is diagonalized. In the absence of magnetism, such anisotropy results in the dispersion relation

$$k_0^2 \equiv \frac{\omega^2}{c^2} = \frac{k_x^2 + k_y^2}{\varepsilon_z} + \frac{k_z^2}{\varepsilon_{x,y}}, \tag{1}$$

which is hyperbolic rather than elliptical [Fig. 1(a)], hence the name of HMMs. A hyperboloidal isofrequency surface is much more extended in the wave-vector space than an ellipsoidal one—indeed, theoretically infinite in the idealization that Eq. (1) holds for all $k_{x,y,z}$—so an HMM supports propagating solutions with very large wave vectors (with k/k_0 greatly exceeding refractive index values typical for naturally occurring dielectrics). These waves, called high-*k* waves for short [1,2], would be evanescent in any natural isotropic or weakly birefringent medium but become propagating in HMMs. The existence of high-*k* waves brings about a rich variety of new physics, both related to the waves themselves (as highly confined information carriers for subwavelength imaging [3]) and associated with a tremendous increase in the photonic density of states in HMMs, resulting in strong modification of all light-matter interaction phenomena that depend on it, such as spontaneous emission [4].

What truly sparked the explosive scientific interest during the past few years was the discovery that HMM functionality can be exhibited in a nonresonant, broadband manner by structures with very simple geometry, such as nanorod arrays [5,6] and metal-dielectric multilayers [1,4,7]. Hyperbolic dispersion was demonstrated experimentally [8], as was an anomalous increase of the decay rate of nearby emitting centers (a broadband Purcell effect) [1,6], along with the direct measurement of radiation enhancement [9]. Many applications of HMMs have been suggested, such as far-field subwavelength imaging or "hyperlensing" [3] and highly absorptive surfaces that benefit (rather than suffer) from increased roughness [7,10], including nanoparticle-induced [11] and internal layer [12] roughness. More fundamental and more intriguing uses for HMMs have also been envisaged, exploiting mathematical similarities between sign changes in the dispersion relation (1) and metric signature transitions in cosmological equations [13,14]. Many more areas of research are being explored, as can be seen in the recent reviews [15–18] and references therein.

Even though the effective permittivity representation of HMMs has proved very successful in predicting and explaining their exotic physics, it is the high-*k* waves that govern the functioning of any HMM on a microscopic level. Hence the high-*k* waves eventually determine the extents and limits of applicability of a particular HMM with respect to any of the effects described above. Thus, it is crucial to understand the physical nature of these waves. In metal-dielectric structures, the conventional wisdom is that the nature is plasmonic, so various groups have chosen different terms for them: *multilayer plasmons* [19], *Bloch plasmon polaritons* [20], or *volume plasmon polaritons* (VPPs) [16,21], which is the term we adopt here. In HMMs with a multilayer geometry, VPPs should arise from coupling of surface plasmon polaritons (SPPs) at layer interfaces [22–24]. In our recent work [2], we showed explicitly that VPPs originate from coupling of short-range SPPs (SRSPPs) in individual metal layers by keeping only the SRSPP response in these layers via a pole expansion.

*sezh@fotonik.dtu.dk

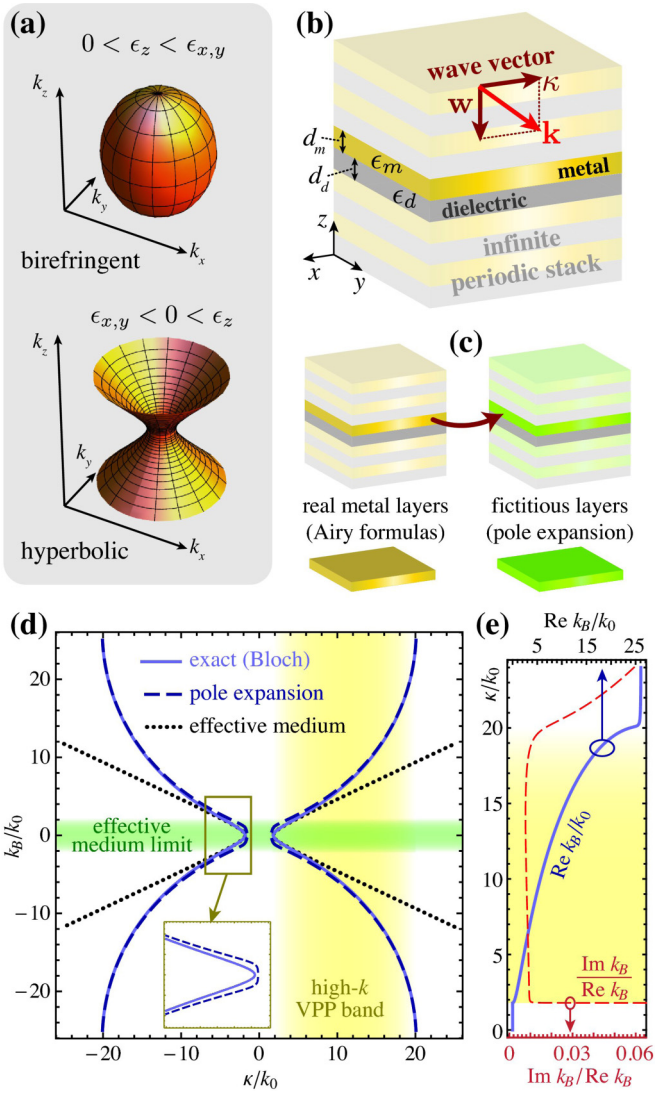

FIG. 1. (Color online) Theoretical background on hyperbolic metamaterials (HMMs). (a) Isofrequency surfaces in the dispersion relation [Eq. (1)] for conventional uniaxial medium ($0 < \varepsilon_z < \varepsilon_{x,y}$) and HMM ($\varepsilon_{x,y} < 0$ and $\varepsilon_z > 0$). (b) An infinite periodic multilayer HMM with geometric notations and wave-vector decomposition used in the paper. (c) The central idea of the paper: the replacement of real metal layers with fictitious layers featuring just a polelike elementary excitation with reflection and transmission coefficients given by Eq. (5). (d) Comparison of the exact multilayer dispersion relation with the one derived from the pole expansion and the effective-medium approximation for the structure with $d_m = 2.3$ nm, $d_d = 11.4$ nm, and $\varepsilon_m = -17.2$, $\varepsilon_d = 2.59$ (relevant for lossless Au/Al_2O_3 structures for $\lambda = 715$ nm [1]; see [2] for more detail). The yellow shaded area shows the band of propagating high-k VPPs. (e) Plots of $\mathrm{Re}\, k_B$ and $\mathrm{Im}\, k_B/\mathrm{Re}\, k_B$ in the VPP band for lossy metal ($\varepsilon_m = -17.2 + 0.8i$).

It is noteworthy that an SRSPP exists for just one value of the wave vector, whereas the resulting VPPs exist in the entire range of them, spanning the isofrequency surface in Fig. 1(a).

Two interesting observations were made alongside this proof. First, it appeared that there is a stark contrast between the two characteristic excitations in the metal layer: the short-range SPP capable of giving rise to HMM behavior, and the long-range SPP (LRSPP) that do not have such a capability. Second, as also mentioned in other accounts [25], VPPs were shown to exist outside of the HMM regime, albeit in a somewhat narrower band in the wave-vector space. The general principle, namely, "the coupling of lower-dimension elementary unit cell excitations forms a higher-dimensional excitation in a periodic arrangement of such cells," is undoubtedly behind the formation of VPPs in multilayer HMMs. Nevertheless, it still remains to be determined what conditions these elementary excitations must satisfy to form a high-k band spanning a broad range of k, such as happens in VPPs. A general understanding would be very useful in determining the applicability range for new types of HMMs, such as, for example, graphene-based multilayers introduced in recent works [26–30].

In this paper, we theoretically investigate general existence conditions for broadband bulk high-k propagating waves (such as VPPs in HMMs) in arbitrary periodic multilayer structures. We treat the elementary excitation in the unit cell of such a structure as a generalized resonance defined by a polelike response in its Fresnel reflection and transmission coefficients. Then, using Bloch's theorem, we derive analytical expressions for the band of high-k propagating solutions that can originate from this elementary excitation by hybridization in the periodic structure. Using these analytical expressions, we show that SRSPPs in thin metal layers can—and commonly do—give rise to HMM-like properties in subwavelength metal-dielectric multilayers; on the other hand, LRSPPs form only a very narrow plasmonic band near the light line of the dielectric and do not produce a high-k band. Furthermore, we apply the formalism to graphene-dielectric metamaterials in the terahertz range. We show that TM-polarized plasmons in individual graphene sheets also hybridize to form VPPs with HMM-like properties in the frequency range where the imaginary part of the graphene conductivity significantly exceeds its real part. On the other hand, *transverse* or TE-polarized graphene plasmons [31,32] behave like LRSPPs in metal-dielectric multilayers, not giving rise to HMM-like behavior.

The present results are primarily valuable from the theoretical point of view, providing a general understanding of how high-k band of bulk propagating waves originate from fixed-k surface excitations in individual layers of a multilayer system. Thus in much of this paper we neglect any losses, so we can focus on the nature of the excitations in the limit where they would persist indefinitely. Nonetheless, our results have practical applications, allowing for very efficient estimation of VPP dispersion and HMM properties in existing HMMs (metal-dielectric and graphene-dielectric multilayers), which is useful in the design of HMM-based devices such as hyperlenses with improved performance. Moreover, the present results provide a means to determine whether any localized excitation (electromagnetic or otherwise) is likely to give rise to HMM-like or bulk-plasmon-like behavior when assembled into a periodic system. Examples may include optical waveguide arrays, multilayers supporting Bloch surface waves or spoof surface plasmons, periodic layers of two-dimensional electron gases (e.g., multiple-quantum-well semiconductor heterostructures), or even acoustic multilayers.

This paper is organized as follows. In Sec. II, we briefly introduce the pole expansion representation [2] for the dispersion relation of multilayer HMMs. We then analyze it on

an abstract level and derive the existence conditions for broad high-k band formation from arbitrary resonant elementary excitation in the metamaterial's unit cell. In Sec. III we apply the derived conditions to several specific cases of pole expansion, including multilayers made of metal and graphene; specifically, we show that short-range SPPs do give rise to HMM behavior while long-range SPPs do not. In Sec. IV, we analyze the effects of losses on the present analysis, and discuss the applicability of graphene for high-k HMMs. Finally, in Sec. V we summarize the results.

II. FORMATION OF A LARGE-WAVE-VECTOR BAND FROM ARBITRARY POLE EXCITATIONS

We begin by recalling the dispersion relation of propagating waves in an infinite periodic metal-dielectric structure where losses are neglected. So metal layers with permittivity $\varepsilon_m < 0$ and thickness d_m alternate with dielectric layers with permittivity $\varepsilon_d > 0$ and thickness d_d [Fig. 1(b)]. Using the standard transfer matrix approach [33], we recall the transfer matrix for one period of the structure,

$$M_1 = \frac{1}{T_m}\begin{bmatrix} T_m^2 - R_m^2 & R_m \\ -R_m & 1 \end{bmatrix}\begin{bmatrix} e^{iw_d d_d} & 0 \\ 0 & e^{-iw_d d_d} \end{bmatrix}, \quad (2)$$

where R_m and T_m are the reflection and transmission coefficients of a metal layer given by the Airy formulas [34]. In a periodic multilayer, Bloch's theorem yields a well-known dispersion relation for TM-polarized waves [22,24,35],

$$\begin{aligned}\frac{\mathrm{Tr}\, M_1}{2} &= \cos[k_B(d_m + d_d)] \\ &= \cos(w_m d_m)\cos(w_d d_d) - \frac{1}{2}\left(\frac{\varepsilon_m w_d}{\varepsilon_d w_m} + \frac{\varepsilon_d w_m}{\varepsilon_m w_d}\right) \\ &\quad \times \sin(w_m d_m)\sin(w_d d_d). \end{aligned} \quad (3)$$

Here $w_{m,d}$ is the normal component of the wave vector in the respective layer:

$$w_m = \sqrt{\varepsilon_m \omega^2/c^2 - \kappa^2}, \quad w_d = \sqrt{\varepsilon_d \omega^2/c^2 - \kappa^2}, \quad (4)$$

where κ is the tangential component of the wave vector. We choose the square root of complex w_j so that $\mathrm{Im}\, w_j \geqslant 0$; if $\mathrm{Im}\, w_j = 0$ we take $\mathrm{Re}\, w_j \geqslant 0$. Equation (3) describes a propagating Bloch wave that reduces to hyperbolic dispersion of Eq. (1) in the limit $w_j d_j \ll 1$ [19].

To relate these Bloch waves to VPPs, one can replace the metal layers with hypothetical systems whose reflection and transmission coefficients contain only one resonant guided-wave excitation, i.e., are of the form of a simple pole [2],

$$T_m = \frac{\tau}{\kappa - \kappa_p}, \quad R_m = \frac{-\tau}{\kappa - \kappa_p} - \frac{\tau}{\kappa_p}, \quad (5)$$

where the location of the pole κ_p and the pole strength τ depend on the exact nature of the excitation and can be determined by fitting Eq. (5) to the exact expressions for R_m and T_m. As shown in our previous work [2], calculating κ_p and τ for the SRSPP in a thin metal layer and substituting Eq. (5) into Eq. (2) results in a modified form of the dispersion relation, which reproduces the exact dispersion relation of the multilayer very closely; an illustrative example involving structures similar to those in earlier studies [2] is shown in Fig. 1(d). Hence, it could be concluded that high-k waves originate from hybridization of SRSPPs in the metal layers, and are indeed VPPs. If there are losses or nonlocalities in the system (e.g., Ohmic losses in metals), the distinction between propagating and evanescent waves becomes more difficult [36,37], as waves both inside and outside the high-k band will have both real and imaginary parts of k_B [11,30]. Nevertheless, the presence of a band with quasipropagating waves is still apparent in the dependence of $\mathrm{Im}\, k_B/\mathrm{Re}\, k_B$ [Fig. 1(e)].

Now we proceed to investigate the mechanism of high-k wave formation in an arbitrary periodic multilayer structure rather than in a metal-dielectric multilayer [Fig. 1(c)]. We revert back to Eq. (5) in its general form, substitute it into Eq. (2), and write the modified dispersion relation as

$$\begin{aligned}&\cos[k_B(d_m + d_d)] \\ &= \frac{\kappa - \kappa_p}{2\tau} e^{2\pi d_d/\lambda\sqrt{\kappa^2 - \varepsilon_d}} - \left[\frac{\tau}{\kappa_p} + \left(\frac{\tau}{\kappa_p}\right)^2 \frac{\kappa - \kappa_p}{2\tau}\right] \\ &\quad \times e^{-2\pi d_d/\lambda\sqrt{\kappa^2 - \varepsilon_d}} \\ &\equiv F(\kappa), \end{aligned} \quad (6)$$

where τ, κ, and κ_p are dimensionless (normalized by $k_0 = \omega/c = 2\pi/\lambda$). The existence condition for propagating solutions will then be

$$F(\kappa) \in [-1; 1]. \quad (7)$$

For convenience in analysis, we further introduce several dimensionless quantities:

$$\xi \equiv \frac{\tau}{\kappa_p}, \quad \eta \equiv \frac{2\pi d_d}{\lambda}, \quad \chi \equiv \frac{\sqrt{\varepsilon_d}}{\kappa_p}, \quad \text{and} \quad \beta \equiv \frac{\kappa}{\kappa_p}. \quad (8)$$

We see that η is the measure of how "subwavelength" the spacer dielectric layers appear to be with respect to the vacuum wavelength of the incident light (so normally $\eta \ll 1$); χ indicates the position of the dielectric cutoff (the point of the light line for a given frequency) normalized to the position of the pole (again, $\chi \ll 1$); ξ characterizes the pole strength (and nothing will be assumed about it so far); and β is the tangential component of the wave vector normalized to the position of the pole. Using these quantities, we can rewrite Eq. (6) in a more symmetric way,

$$\tfrac{1}{2}(\beta - 1)A(\beta) - \tfrac{1}{2}(\beta + 1)A^{-1}(\beta) \equiv F(\beta) \in [-1; 1], \quad (9)$$

where

$$A = \xi^{-1}\exp(\eta\kappa_p\sqrt{\beta^2 - \chi^2}). \quad (10)$$

Although Eqs. (9) and (10) are sufficient for a fast numerical prediction of where the high-k band would be for all possible combinations of β and ξ (see Fig. 2), it is instructive to study the limiting cases of Eq. (9). For a combination of parameters such that $A \gg 1$ (achieved for significantly large κ_p and/or very small ξ), one can neglect the term with A^{-1} and see that $F(\beta) = \pm 1$ can be solved analytically to yield

$$\beta = 1 + (\eta\kappa_p)^{-1} W(\pm 2\xi\eta\kappa_p e^{-\eta\kappa_p}), \quad (11)$$

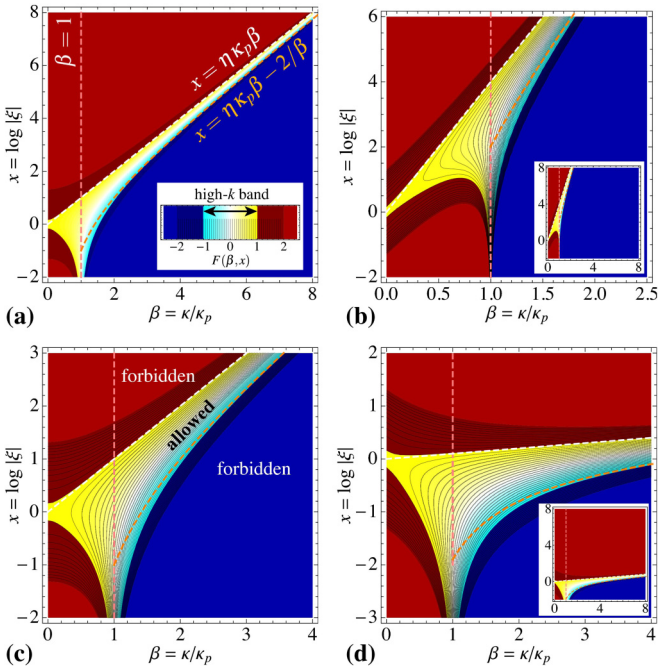

FIG. 2. (Color online) Behavior of Eq. (9) in different regimes. Light colors (cyan to white to yellow) correspond to the area where $-1 < F < 1$ and propagating high-k waves exist; dark colors (dark red and blue) indicate regions where $|F| > 1$ and high-k wave propagation is forbidden. (a) Illustration of the limiting behavior of $F(\beta,x = \ln|\xi|)$ for large β and x; the dashed lines show the asymptotes given by Eqs. (12) and (13). (b)–(d) An enlarged view of $F(\beta,x)$ around the asymptote intersection point ($\beta = 1, x = \eta\kappa_p$) for $\eta\kappa_p$ equal to (b) 4, (c) 1, and (d) 0.1. The insets show the plots in (b) and (d) in the same scale as (a) for comparison.

where $W(z)$ is the Lambert W function [38] defined as the solution of $W(z)e^{W(z)} = z$. If its argument is small, we can use the first-order approximation $W(z) \approx z$ to yield that high-k waves exist if

$$\beta \in [1 - 2\xi e^{-\eta\kappa_p};\ 1 + 2\xi e^{-\eta\kappa_p}]. \tag{12}$$

So, in the limit of small pole strength ξ, propagating waves are observed around the pole excitation that gives rise to them, i.e., there is a high-k band around $\beta = 1$ (i.e., $\kappa = \kappa_p$). This band is usually narrow, and it gets progressively narrower as ξ decreases, so the line $\beta = 1$ represents the limiting behavior of Eq. (9) as $\xi \to 0$. Physically, this means that an excitation represented by a pole which is infinitely weak gives rise to only a single wave with $\kappa = \kappa_p$. On the other hand, Eq. (12) shows that the band widens if $\eta\kappa_p$ gets smaller, e.g., as the structure becomes more subwavelength (smaller η).

It is still not clear, however, how the band of propagating waves can fill a very broad range of κ. Doing so requires violating the assumptions leading to Eq. (12) and considering the other limit of Eq. (9). Namely, we notice that for the case $A = A^{-1} = 1$, we have $F(\beta) = -1$ regardless of any other parameters. Changing to the logarithmic scale with respect to ξ by defining $x \equiv \ln|\xi|$, we see that the dependence

$$x = \eta\kappa_p\beta \quad \text{where } e^x = |\xi| \tag{13}$$

is exactly at the edge of the high-k band. Indeed, if the argument of the exponent in Eq. (10) is small enough so that $A^{\pm 1} \approx 1 \pm (\eta\kappa_p\beta - x)$, then it follows that $F(\beta) = 0$ for $x = \eta\kappa_p\beta - 1/\beta$ and $F(\beta) = 1$ for $x = \eta\kappa_p\beta - 2/\beta$ [see Fig. 2(a)]. Hence Eq. (13) describes the second limiting case for the existence of the high-k band. Unlike in the previous case, the band now occurs for much larger κ than the pole location κ_p, which is indicative of very strong coupling between polelike resonances in the neighboring fictitious layers due to a very large ξ. Interestingly, this high-k band also gets progressively narrower as ξ increases, converging to the line in Eq. (13) as $\xi \to \infty$. The reason is that very strong resonators and the associated very strong coupling between them make the states with different Bloch wave numbers degenerate to a single collective state.

This limiting case analysis makes it especially easy to predict the region of existence for the high-k band in the (β,x) space, as seen in Fig. 2; this plot can be regarded as a general graphical solution of Eq. (9) for all possible values of the resonant pole location and strength. We see that as the excitation becomes stronger (ξ increases), the band follows the line $\beta = 1$ and grows wider. This behavior continues until $x = 0$, after which the band slants to follow the line $\beta = x/(\eta\kappa_p)$. The region where the two asymptotes overlap near the intersection point ($\beta = 1, x = \eta\kappa_p$) is where Eq. (9) ceases to be analytically solvable and the band has a more complicated shape [Figs. 2(b)–2(d)].

We can thus identify two distinct characteristic cases when the high-k band is sufficiently broad. First, it can be seen that for both the limiting cases, the band widens as ξ approaches unity (Fig. 2). Hence the region $0.1 \leqslant \xi \leqslant 10$ corresponds to the case when bulk propagating solutions are supported for the widest range of κ. Second, for the special case $\eta\kappa_p \ll 1$, when the line corresponding to Eq. (13) is nearly horizontal, there is a narrow range of $x \in [-2/\beta; 0]$ when propagating waves exist for β from below unity all the way to $\sqrt{2/(\eta\kappa_p)}$, approaching very large values for $x \to -0$ for deeply subwavelength structures. This provides convergence of the presented analysis to the effective-medium limit for $\eta \to 0$. It is also established that nonzero ζ (i.e., variation of the permittivity of the spacer layers ε_d) influences the general solution only weakly, suppressing the existence of propagating waves below the light line ($\beta \leqslant \chi$ or $\kappa \leqslant \sqrt{\varepsilon_d}$) and slightly modifying the limiting behavior near it.

It is important to stress that Fig. 2 describes the behavior of multilayered HMM-like metamaterials *regardless* of the specific physical mechanism of the single-layer excitation captured by Eq. (5). To apply these results to a case relevant in practice, where the pole expansion would correspond to a specific physical excitation such as a surface plasmon, the first step is to calculate the actual expressions for κ_p and ξ for that kind of excitation. Then the intersection between the lines $F(\beta,x) = \pm 1$ and $x = \ln|\xi|$ would produce the two points $\beta_\pm$, with the values $\kappa_\pm = \kappa_p\beta_\pm$ denoting the edges of the high-k band. Modifying the graphical solution in Fig. 2 in such a way that the ordinate axis shows some physical parameter that affects x in a given physical system (such as frequency in multilayers made of dispersive materials [30]), rather than x itself, would provide an overview of the high-k band properties in that particular system.

III. EXAMPLES

A. Metal-dielectric multilayers

The most straightforward way to test the proposed existence criteria is to apply the conditions to the well-studied HMM produced from metal-dielectric multilayers, using SPPs in the metal layers as the elementary excitations in Eq. (5). It is known that a metal layer supports two types of such plasmons depending on whether the individual plasmons at the layer interfaces are coupled symmetrically or antisymmetrically with respect to the dominant field component E_z. Both these modes can be obtained from the equation (r_{md} is the Fresnel reflection coefficient at the metal-dielectric interface)

$$1 - r_{md}^2 \exp(2i w_m d_m) = 0, \tag{14}$$

The primary difference between them is the behavior of their propagation constant κ_p as the metallic layer thickness d_m approaches zero. The symmetrically coupled SPP has its wave vector approach the light cone ($\kappa_p \to \sqrt{\varepsilon_d}$), and if the metal is lossy, the losses decrease as the wave becomes increasingly less confined to the layer. The asymmetrically coupled SPP has its wave-vector approach infinity ($\kappa_p \to \infty$), and the wave becomes increasingly more confined to the metal layer, so the losses increase. For the latter reason, these two SPPs are traditionally referred to as long-range and short-range SPPs, respectively.

It has already been proved [2] that SRSPPs can and do give rise to the high-k VPP band in metal-dielectric HMMs, and we begin by reproducing this result with the proposed criteria. In the appropriate limit of a sufficiently thin metal layer, the expressions for the pole expansion parameters for Eq. (5) can be obtained from Eq. (14) as, in dimensionless units,

$$\kappa_p = \frac{\ln|r|}{2\pi d_m/\lambda}, \quad \tau = \frac{r^{-1} - r}{2(2\pi d_m/\lambda)}, \qquad r = \lim_{\kappa\to\infty} r_{md} = \frac{\varepsilon_m - \varepsilon_d}{\varepsilon_m + \varepsilon_d}. \tag{15}$$

We note at once that ξ does not depend on d_m, making the analysis particularly easy:

$$\xi = \frac{r^{-1} - r}{2\ln|r|} = \frac{2f}{(f^2-1)\ln\left|\frac{1+f}{1-f}\right|}, \tag{16}$$

where $f = -\varepsilon_d/\varepsilon_m$. We can see that $\xi \gtrsim 1$ unless $f \to 1$ [Fig. 3(a)]. So it can be concluded that broadband VPPs are commonly formed by hybridization of SRSPPs, as confirmed by the example in Fig. 3(b) with x taken from Fig. 3(a). The only exception is when $\varepsilon_m + \varepsilon_d \approx 0$ leading to $|\xi| \gg 1$, so the VPP band becomes increasingly more narrow and moves towards larger κ [see the inset in Fig. 2(b)]. Note that this corresponds to an epsilon-near-zero (ENZ) regime rather than an HMM regime, and the narrowing and shifting of the VPP band near the ENZ points is consistent with our earlier observation [2]. The VPP band shift remains small since the slope parameter $\eta\kappa_p = (d_d/d_m)\ln|r|$ becomes very large in the ENZ case.

On the other hand, the LRSPP is obtained from Eq. (14) by considering the other limit ($\kappa_p \to \sqrt{\varepsilon_d}$). The resulting

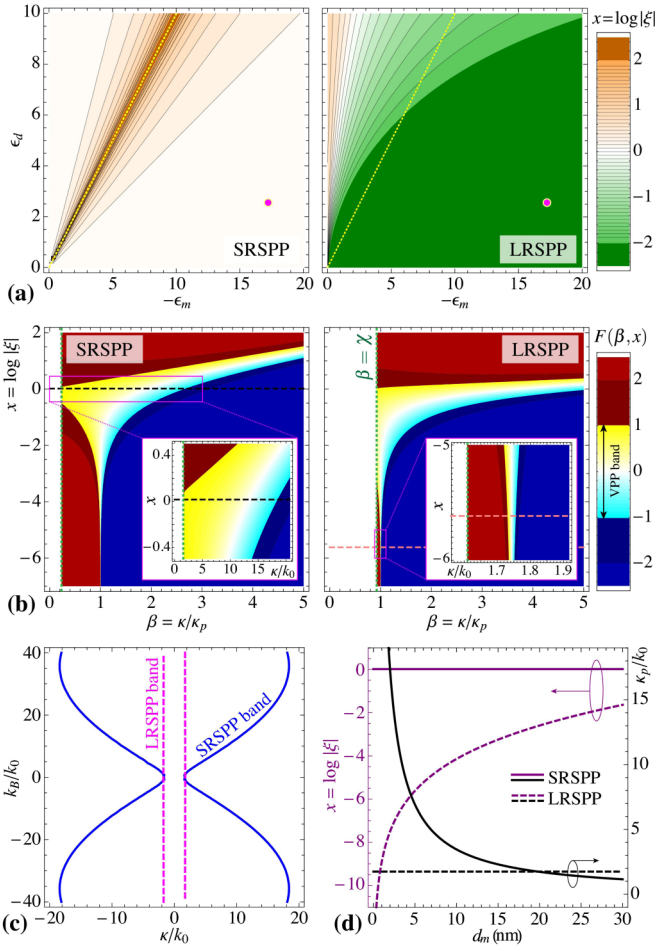

FIG. 3. (Color online) Formation of the VPP band in metal-dielectric HMMs from SRSPPs and LRSPPs. (a) Dependence of x on the permittivities of metal and dielectric in a thin metal layer ($d_m = 5$ nm) for SRSPPs and LRSPPs; the dotted line corresponds to $f = 1$. (b) Example dependencies of $F(\beta,x)$ for SRSPPs and LRSPPs in a structure with $d_m = d_d = 5$ nm and material parameters as in Fig. 1(c). The insets show the enlarged view on the scale of $\kappa_p/(\omega/c)$. (c),(d) Comparison between SRSPP and LRSPP cases for (c) the dispersion relation of the VPP band and (d) the dependence of κ_p and x on d_m. The values for x for plots in (b) are taken from the plots in (a) at the corresponding values of parameters (shown as a dot).

expressions are

$$\kappa_p = \sqrt{\varepsilon_d + (\varepsilon_d - \varepsilon_m)\frac{\varepsilon_d^2}{\varepsilon_m^2}\left(\frac{1-\delta}{1+\delta}\right)^2}, \qquad \tau = \frac{\varepsilon_d - \varepsilon_m}{2\kappa_p}\frac{\varepsilon_d^2}{\varepsilon_m^2}\frac{(\delta-1)^2}{\delta(\delta+1)}, \quad \delta = e^{-d_m\sqrt{(\varepsilon_d-\varepsilon_m)}}, \tag{17}$$

which gives

$$\xi = \frac{(\varepsilon_d - \varepsilon_m)\varepsilon_d^2/\varepsilon_m^2}{\varepsilon_d + (\varepsilon_d - \varepsilon_m)\frac{\varepsilon_d^2}{\varepsilon_m^2}\left(\frac{1-\delta}{1+\delta}\right)^2}\frac{(\delta-1)^2}{\delta(\delta+1)}, \tag{18}$$

and it can be seen that $\xi \to 0$ as $d_m \to 0$ and the structure becomes increasingly more subwavelength. This means that LRSPPs hybridize to form but a very narrow band around κ_p

according to Eq. (12) [Fig. 2(a)], and thus do not contribute to the VPP band. This is seen in Fig. 3(a), and further demonstrated by comparing the location of the area given by $-1 < F(\beta,x) < 1$ in the (β,x) coordinates for the characteristic metal-dielectric multilayers [Fig. 3(b)] and the dispersion of VPPs in the bands [Fig. 3(c)] for LRSPP vs SRSPP cases. We reiterate here that $x = \ln|\xi|$ is given by Eqs. (16) and (18) rather than chosen arbitrarily. This result can also be explained by noting that an LRSPP in a metallic layer bears more and more resemblance to a plane wave in the surrounding medium as the layer becomes thinner, which is accompanied by progressively poorer coupling between the wave and the metal; it is this poor coupling that manifests itself in $\xi \to 0$. The same poor coupling will thus be characteristic for VPPs resulting from LRSPPs, which will therefore be very similar in properties to plane waves propagating in the dielectric of the HMM, and thus occupy but a very narrow range of κ.

On the other hand, for ξ to be on the order of unity in the LRSPP case, the quantity $2\pi d_m/\lambda$ needs to be between 0.25 and 1 [see Fig. 3(d)], i.e., the multilayer should not be very subwavelength. In this regime, it can be expected that both LRSPPs and SRSPPs may contribute to the VPP band, in line with the recent observation that real multilayer structures can outperform ideal HMMs for some values of layer thicknesses [34,39].

B. Graphene-dielectric multilayers

Besides metallic layers, plasmonic excitations are present in other thin-film structures such as graphene (see the recent tutorial review [40] and references therein), and it has been proposed that separating graphene layers by dielectric spacers and combining them into multilayers [41,42] can give rise to a new type of HMM, predominantly in the THz range [26–29]; the recent study by Othman *et al.* [30] specifically shows the existence of propagating high-k waves in a broad parameter window. Here we apply our approach to analyze the prerequisites needed for the VPP band formation.

Graphene can be regarded as an infinitely thin sheet with surface conductivity σ. In the THz to far infrared (far-IR) range for graphene Fermi energy $E_F > k_B T$ (k_B being the Boltzmann constant), it can be calculated according to the Kubo approach with the formula [43]

$$\sigma = i\frac{e^2 k_B T}{\pi\hbar^2}\left[\frac{E_F}{k_B T} + 2\ln(1+e^{-E_F/k_B T})\right]\frac{1}{\omega+i\gamma} + i\frac{e^2}{4\pi\hbar}\ln\frac{2|E_F| - \hbar(\omega+i\gamma)}{2|E_F| + \hbar(\omega+i\gamma)}, \tag{19}$$

where T is the temperature and γ is the damping rate, which depends on the quality of the graphene. The first and the second terms in Eq. (19) correspond to intraband and interband contributions, respectively. This expression is generally found to be accurate, even though corrections can be introduced in special cases (see, e.g., [44] and references therein).

The resulting conductivity (real and imaginary parts) is shown in Figs. 4(a) and 4(b). We see that the imaginary part $\mathrm{Im}\,\sigma > 0$, which corresponds to "metal-like" behavior of graphene, everywhere except in a narrow region of frequencies and electrochemical potentials [white area close to the dashed line in Fig. 4(b)]. As with the metal-dielectric multilayers, we will neglect losses for now, considering the frequency range where the real part of σ is small, and will assume that σ is purely imaginary.

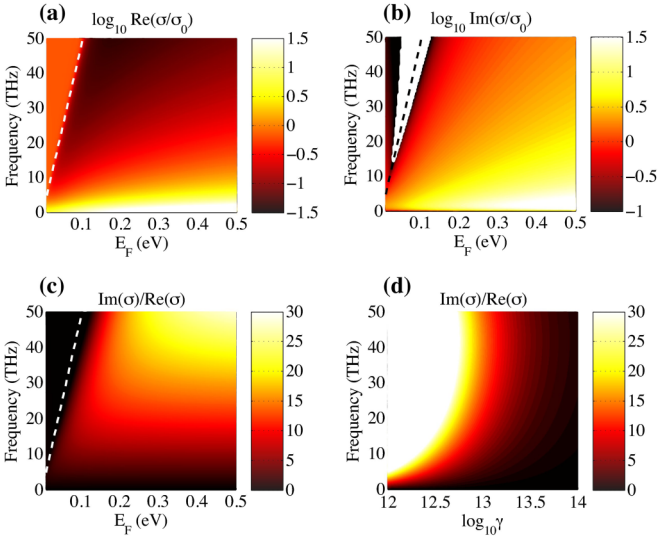

FIG. 4. (Color online) Graphene conductivity σ in units of the elementary conductivity $\sigma_0 = e^2/4\hbar = 0.061$ mS in logarithmic scale. (a) Real and (b) imaginary part, depending on frequency ω and electrochemical potential (Fermi level) E_F. The dashed line corresponds to the Pauli blocking limit $\hbar\omega = 2E_F$. The white region around the dashed line in (b) corresponds to the region of negative $\mathrm{Im}\,\sigma$. Also shown is the figure of merit (FOM) $\mathrm{Im}\,\sigma/\mathrm{Re}\,\sigma$ dependence on frequency and (c) E_F for the damping $\gamma = 10^{13}$ s^{-1}; (d) on the damping γ for the fixed Fermi level $E_F = 0.2$ eV. We consider the regions with FOM greater than zero suitable for HMMs.

Surrounding a sheet of graphene with conductivity σ by dielectric with permittivity ε, the transmission coefficient for the TM polarization is given by [45]

$$T = \frac{2\varepsilon/\sqrt{\varepsilon-\kappa^2}}{2\varepsilon/\sqrt{\varepsilon-\kappa^2} + (Z_0\sigma)}, \tag{20}$$

where $Z_0 = 1/(\varepsilon_0 c) \approx 377\ \Omega$ is the impedance of free space. Introducing $S \equiv 2\varepsilon/(Z_0\mathrm{Im}\,\sigma)$, Eq. (20) yields the expressions for the pole expansion coefficients

$$\kappa_p = \sqrt{\varepsilon+S^2}, \quad \tau = -\frac{S^2}{\sqrt{\varepsilon+S^2}}, \quad \xi = -\frac{S^2}{\varepsilon+S^2}. \tag{21}$$

It is remarkable that realistic graphene conductivities in the range $\mathrm{Im}\,\sigma < 100e^2/(4\hbar)$ yield large values of S between 1 and 100. Since $|\xi|$ tends to unity for large S, it turns out to be between 0.1 and 1, which is favorable for the VPP band to be broad and pronounced, in a large parameter window, as shown in Fig. 5(a). Changing the Fermi level allows the tuning of conductivity to the desired value [see Fig. 4(b)] while maintaining the deeply subwavelength thickness of such layers for THz frequencies; Fig. 5(b) additionally confirms the presence of a VPP band in such graphene-dielectric multilayers. These results agree with the study of Othman *et al.*, predicting the existence of Bloch propagating waves in graphene-dielectric multilayers in the hyperbolic dispersion regime [30] and confirm the emergence of VPPs in graphene

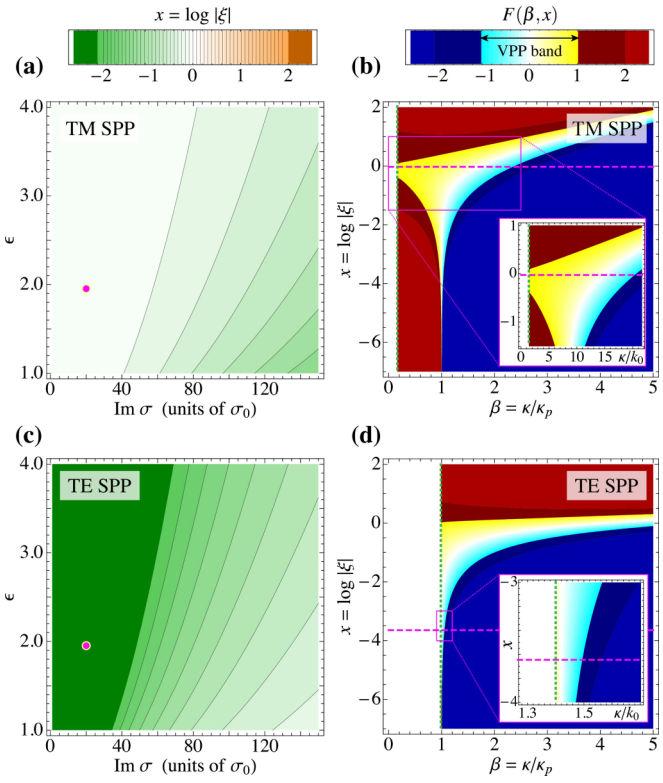

FIG. 5. (Color online) Formation of the VPP band in graphene HMMs. (a) The dependence of x on graphene conductivity and dielectric layer permittivity. (b) Same as Fig. 3(b) for graphene multilayers with $\sigma = 20i\sigma_0$ [where $\sigma_0 = e^2/(4\hbar)$], $d = 5$ nm, and $\varepsilon = 1.96$. (c),(d) Same as (a),(b) but for TE-polarized graphene plasmons. The values for x for plots in (b),(d) are taken from the plots in (a),(c) at the corresponding values of parameters (shown as a dot).

from TM plasmons present in graphene monolayers. Note that in the present approach the parameter window for the high-k band can be identified without regard for the curvature of its dispersion relation, i.e., regardless of whether or not the multilayer has hyperbolic dispersion.

The key difference between VPPs in metal-dielectric and graphene multilayers is that in the former $\xi \gtrsim 1$ while in the latter $\xi \lesssim 1$. As a result, metal-dielectric layers benefit from a decrease of $\eta\kappa_p$ (e.g., by decreasing d_d and making the structure more subwavelength), whereas for graphene multilayers this is less relevant because the slanted branch of $F(\beta,x) \in [-1;1]$ is outside of the working values of $x < 0$.

It was also pointed out recently that in addition to conventional SPPs for TM-polarized waves, graphene supports transverse TE-polarized SPPs [31,32] in a narrow range of parameters where $\mathrm{Im}\,\sigma < 0$ and $\mathrm{Re}\,\sigma$ is small. It is interesting to analyze whether these SPPs can give rise to HMM-like behavior. The TE counterparts to Eqs. (20) and (21) are

$$T' = \frac{2\sqrt{\varepsilon - \kappa^2}}{2\sqrt{\varepsilon - \kappa^2} + (Z_0\sigma)}, \tag{22}$$

and (introducing $Q \equiv Z_0|\mathrm{Im}\,\sigma|/2$)

$$\kappa_p' = \sqrt{\varepsilon + Q^2}, \quad \tau' = \frac{Q^2}{\sqrt{\varepsilon + Q^2}}, \quad \xi' = \frac{Q^2}{\varepsilon + Q^2}. \tag{23}$$

Here we note that TE-polarized plasmons exist only very close to the singularity point in the graphene conductivity, with realistic $|\mathrm{Im}\,\sigma| < 2e^2/(4\hbar)$. Hence Q is a small quantity on the order of 0.05, making κ_p' very close to $\sqrt{\varepsilon}$ and $\xi' \ll 1$. This makes TE-polarized plasmons in graphene much like LRSPPs, which hybridize only into an extremely narrow VPP band, as can indeed be seen in Figs. 5(c) and 5(d).

IV. INFLUENCE OF LOSSES

So far, we have completely neglected the effects of losses in our analysis. While this idealization was necessary to be able to rigorously define the band of propagating high-k band and to determine its shape in the parameter space analytically, this idealization is certainly not always compatible with practical considerations. Indeed, losses in metals are not always negligible, especially at visible frequencies (the operating range for many multilayer HMMs), and losses in graphene are certainly non-negligible and highly dependent on the graphene quality [as seen in Fig. 4(a), the real part of the conductivity can be quite significant].

Therefore, to complete the present analysis, it is worthwhile to explore the influence of losses on the propagating characteristics of high-k waves in the generalized multilayers considered here. While we realize that addressing the question of high-k wave propagation in lossy multilayers is beyond the scope of the present paper and warrants a separate analysis, we try to establish the applicability limits of the proposed lossless analysis to systems with minor losses, and confirm its applicability to the considered cases of metal-dielectric and graphene-dielectric multilayers.

A reasonable way to incorporate losses into a resonant excitation captured by the pole expansion in Eq. (5) is via a damping term in the denominator, or, in other words, by moving the pole point κ_p away from the real axis in the complex plane. As a result, the coefficients in Eq. (6) become complex, and the distinction between propagating and evanescent Bloch waves can no longer be rigorously made. We can, however, introduce the "performance metric" for the Bloch waves, defined as the ratio between its propagation and attenuation constant [30] as $\rho = \mathrm{Re}\,k_B/\mathrm{Im}\,k_B = \mathrm{Re}\arccos F/\mathrm{Im}\arccos F$, with higher values meaning that the wave is able to propagate more effective wavelengths before it is fully damped.

The resulting plots of this propagation-to-attenuation ratio for the same conditions as in Fig. 2(c) with varying amount of damping in the pole expansion are shown in Fig. 6(a). We see that when the losses are minor (with $\mathrm{Im}\,\kappa_p/\mathrm{Re}\,\kappa_p < 0.005$), the area with $\rho \neq 0$ almost fully coincides with the shape of the high-k band for the lossless case as in Fig. 2(c) with the exception that the edges of the band are smeared, in line with earlier predictions [34,36]. Increasing the amount of losses makes the smearing more pronounced and affects ρ in some parts of the high-k band more strongly than in others. This reduces the useful width of the high-k band in practice, compared to the lossless case, especially for lower values of ξ. Nevertheless, we see that the shape of the area where high-k waves display *some* propagating character still coincides with the predictions of the lossless model, with ρ remaining sufficiently high.

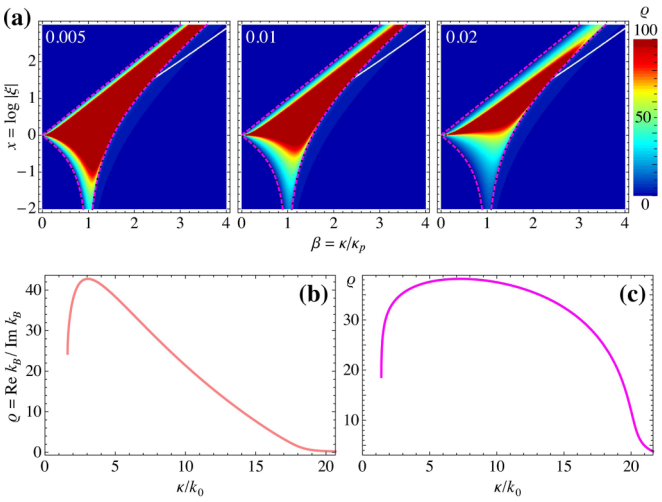

FIG. 6. (Color online) (a) Propagation-to-attenuation ratio for the high-k propagating waves, defined as $\rho = \mathrm{Re}\, k_B/\mathrm{Im}\, k_B = \mathrm{Re}\arccos F/\mathrm{Im}\arccos F$ as in Ref. [30], for the same conditions as in Fig. 2(c) for complex κ_p with $\mathrm{Im}\,\kappa_p/\mathrm{Re}\,\kappa_p$ equal to 0.005, 0.01, and 0.02. Dashed lines denote the contour of the high-k band in the lossless case. (b),(c) Similarly defined ρ for (b) SRSPP excitations in metal-dielectric multilayer with realistic metal losses and (c) TM plasmon excitations in graphene-dielectric multilayers with $\sigma/\sigma_0 = 0.75 + 20i$ (FOM of 26.7) and other parameters similar to the insets in Fig. 3(b) and Fig. 5(b), respectively, and calculated along the horizontal dashed line in those insets.

With this result in mind, the predictions of the lossless model about where one should look for propagating high-k waves can be regarded as accurate, at least for $\mathrm{Im}\,\kappa_p/\mathrm{Re}\,\kappa_p$ up to about 0.02, while for higher losses the results can be regarded as a guideline, and the precise characteristics of bulk propagating waves should be established by additional calculations. Since losses work to reduce, and never to enlarge, the effective width of the high-k band, the conclusion that the values of ξ should be near unity remains important in the lossy case.

We have also calculated the propagation-to-attenuation ratio ρ for the VPP waves predicted for the considered examples of metal-dielectric and graphene-dielectric multilayers [Figs. 3(b) and 5(b), respectively]. In that case, we have used complex values of ε_m and σ, respectively, to directly solve Eq. (6) for the specific examples. The results, shown in Figs. 6(b) and 6(c), confirm that even though ρ varies throughout the VPP band quite significantly, it remains of the order of several tens.

To further discuss the parameter range where the present analysis is applicable to graphene-dielectric multilayers, we introduce the figure-of-merit (FOM) $\mathrm{Im}\,\sigma/\mathrm{Re}\,\sigma$, which is an adaptation of the quantity commonly used to characterize the amount of losses in metamaterials to a single graphene sheet. We will assume that losses in graphene are small if the FOM is greater than 10. Figure 4(c) presents the figure of merit for the damping value $\gamma = 10^{13}$ s^{-1} seen in literature [46]. As we see, a FOM greater than 10 corresponds to the Fermi level $E_F > 0.15$ eV and frequencies above 20 THz, whereas in the lower THz and microwave range graphene is essentially just a dissipative layer (resistor). We should keep in mind that at photon energies larger than 0.2 eV, which correspond to the frequencies above 50 THz, the interaction with the lattice phonons [47] in the graphene and dielectric spacer layers in multilayered graphene introduce additional large losses not taken into account in Eq. (19). Therefore the region from 20 to 50 THz is probably the best for the realization of graphene-based HMMs, and larger E_F are favorable for better HMM performance.

Another parameter, namely, damping (or collision frequency) γ, depends very much on the quality of graphene (its growth process and handling when transferring to the substrate). The values reported in the literature vary widely from 10^{12} to 10^{14} s^{-1} (the reader is referred to the recent review of graphene for THz applications [46]). In Fig. 4(d) the influence of damping on the figure of merit is demonstrated. Whereas for the above-mentioned $\gamma = 10^{13}$ s^{-1} graphene could be used for an HMM only starting from 20 THz, reducing the damping by ten times ($\gamma = 10^{12}$ s^{-1}) makes graphene HMMs feasible starting from as low as 1.6 THz. On the other hand, doubling the damping to $\gamma = 2 \times 10^{13}$ s^{-1} makes graphene useless for building HMMs in the entire THz-IR range. However, there are definite grounds for optimism in the constant progress in graphene fabrication technology. For example, chemical vapor deposition growth of centimeter-large monocrystalline graphene with quality rivaling that of exfoliated graphene [48], and large mobility of carriers in graphene surrounded by two-dimensional boron nitride [49] have been reported recently.

It should be noticed, though, that the discussion on the optimization of losses in HMMs is relevant to only some, but not all, applications of HMMs. Fot those applications that require reasonable transmission coefficients, such as hyperlensing [3], losses should be as small as possible. For some other applications, such as HMM-based absorbers [7,11], large losses are quite tolerable and even desirable.

V. CONCLUSIONS AND OUTLOOK

In summary, we have investigated the general theoretical conditions for an arbitrary elementary excitation existing in the unit cell of a multilayer periodic system to hybridize into broadband bulk high-k propagating waves (such as VPPs in HMMs). By isolating the unit cell elementary excitation in the form of a generalized resonance defined by a polelike response in its Fresnel reflection and transmission coefficients [Eq. (5)], and by using Bloch's theorem to couple the unit cells via dielectric spacer layers, we have derived analytic relations connecting the width of the resulting band of propagating waves in the k space with the properties of the elementary excitations, such as the pole location and strength, as well as parameters of the dielectric spacer layers.

Using these analytical expressions, we have confirmed that one kind of surface plasmon existing in thin metal layers, namely, the SRSPPs, can and normally do give rise to a broad band of volume plasmon polaritons, resulting in HMM-like properties of subwavelength metal-dielectric multilayers [2]. Conversely, the other kind of SPP in such layers, namely, the LRSPPs, form only a very narrow plasmonic band near the light line of the dielectric and do not produce a broad high-k band.

We have also applied the formalism to multilayered graphene-dielectric metamaterials in the THz range and shown that TM-polarized plasmons in individual graphene sheets do hybridize to form VPPs with HMM-like properties, and the VPP band is broadband enough for realistic values of graphene conductivity [for the considered geometry $\mathrm{Im}\,\sigma < 100e^2/(4\hbar)$]. On the other hand, transverse (TE-polarized) graphene plasmons form only a very narrow VPP band, not giving rise to HMM properties and behaving like LRSPPs in this respect. We have also shown that graphene can be a good building material for high-k band THz and IR metamaterials, if it has sufficiently high quality (the damping γ smaller than 2×10^{13} s^{-1}).

Along with providing a general theoretical understanding of the formation of a high-k band of bulk propagating waves from fixed-k surface excitations in individual layers of a multilayer system, our results have promising practical applications. They are twofold. First, the analytic expressions allow for very easy and computationally efficient estimations of VPP dispersion in existing metal-dielectric and graphene multilayer HMMs, which can be used to design HMMs with optimized performance. Second, on a more abstract level, the formalism provides insight into the general question of whether the broadband large-wave-vector higher-dimensional response should be expected from *any* given type of lower-dimensional elementary excitations in *arbitrary* periodic systems, not necessarily bilayer unit cells, but also many-layer and gradient systems. Examples may include new types of photonic structures such as waveguide arrays and multilayers based on Bloch surface waves or spoof surface plasmons. Moreover, by virtue of mathematical similarities between electromagnetic waves and other wave phenomena in physics (such as acoustic waves in elastic multilayers and steady-state solutions of the Schrödinger equation in multiple-quantum-well heterostructures), it can be speculated that the present results may be applied to these alternative systems, extending the metamaterial approach beyond electromagnetism.

ACKNOWLEDGMENTS

The authors thank I. Iorsh for helpful suggestions. S.V.Z. acknowledges financial support from the People Programme (Marie Curie Actions) of the European Union's 7th Framework Programme, FP7-PEOPLE-2011-IIF, under REA Grant Agreement No. 302009 (Project HyPHONE). A.A. acknowledges financial support from the Danish Council for Technical and Production Sciences through the GraTer Project (Grant No. 0602-02135B). J.E.S. acknowledges financial support from the Natural Sciences and Engineering Research Council of Canada.

[1] Z. Jacob, J.-Y. Kim, G. V. Naik, A. Boltasseva, E. E. Narimanov, and V. M. Shalaev, Appl. Phys. B **100**, 215 (2010).
[2] S. V. Zhukovsky, O. Kidwai, and J. E. Sipe, Opt. Express **21**, 14982 (2013).
[3] Z. Jacob, L. V. Alekseyev, and E. Narimanov, Opt. Express **14**, 8247 (2006).
[4] Z. Jacob, I. I. Smolyaninov, and E. E. Narimanov, Appl. Phys. Lett. **100**, 181105 (2012).
[5] M. A. Noginov, Yu. A. Barnakov, G. Zhu, T. Tumkur, H. Li, and E. E. Narimanov, Appl. Phys. Lett. **94**, 151105 (2009).
[6] M. A. Noginov, H. Li, Yu. A. Barnakov, D. Dryden, G. Nataraj, G. Zhu, C. E. Bonner, M. Mayy, Z. Jacob, and E. E. Narimanov, Opt. Lett. **35**, 1863 (2010).
[7] J. Liu, G. V. Naik, S. Ishii, C. DeVault, A. Boltasseva, V. M. Shalaev, and E. Narimanov, Opt. Express **22**, 8893 (2014).
[8] T. S. Luk, I. Kim, S. Campione, S. W. Howell, G. S. Subramania, R. K. Grubbs, I. Brener, H.-T. Chen, S. Fan, and M. B. Sinclair, Opt. Express **21**, 11107 (2013).
[9] J. Kim, V. P. Drachev, Z. Jacob, G. V. Naik, A. Boltasseva, E. E. Narimanov, and V. M. Shalaev, Opt. Express **20**, 8100 (2012).
[10] E. E. Narimanov, H. Li, Y. A. Barnakov, T. U. Tumkur, and M. A. Noginov, Opt. Express **21**, 14956 (2013).
[11] C. Guclu, S. Campione, and F. Capolino, Phys. Rev. B **86**, 205130 (2012).
[12] A. Andryieuski, S. V. Zhukovsky, and A. V. Lavrinenko, Opt. Express **22**, 14975 (2014).
[13] I. I. Smolyaninov and E. E. Narimanov, Phys. Rev. Lett. **105**, 067402 (2010).
[14] I. I. Smolyaninov and Yu-Ju Hung, J. Opt. Soc. Am. B **28**, 1591 (2011).
[15] C. L. Cortes, W. Newman, S. Molesky, and Z. Jacob, J. Opt. **14**, 063001 (2012).
[16] V. Drachev, V. A. Podolskiy, and A. V. Kildishev, Opt. Express **21**, 15048 (2013).
[17] A. Poddubny, I. Iorsh, P. Belov, and Yu. Kivshar, Nat. Photon. **7**, 948 (2013).
[18] A. A. Orlov, I. V. Iorsh, S. V. Zhukovsky, and P. A. Belov, Photon. Nanostruct. Fundam. Appl. **12**, 213 (2014).
[19] J. Schilling, Phys. Rev. E **74**, 046618 (2006).
[20] I. Avrutsky, I. Salakhutdinov, J. Elser, and V. Podolskiy, Phys. Rev. B **75**, 241402(R) (2007).
[21] S. Ishii, A. V. Kildishev, E. Narimanov, V. M. Shalaev, and V. P. Drachev, Laser Photon. Rev. **7**, 265 (2013).
[22] S. Feng, J. M. Elson, and P. L. Overfelt, Opt. Express **13**, 4113 (2005).
[23] B. Wood, J. B. Pendry, and D. P. Tsai, Phys. Rev. B **74**, 115116 (2006).
[24] G. Rosenblatt and M. Orenstein, Opt. Express **19**, 20372 (2011).
[25] A. A. Orlov, P. M. Voroshilov, P. A. Belov, and Yu. S. Kivshar, Phys. Rev. B **84**, 045424 (2011).
[26] A. Andryieuski, A. V. Lavrinenko, and D. N. Chigrin, Phys. Rev. B **86**, 121108 (2012).
[27] I. V. Iorsh, I. S. Mukhin, I. V. Shadrivov, P. A. Belov, and Yu. S. Kivshar, Phys. Rev. B **87**, 075416 (2013).
[28] K. V. Sreekanth, A. De Luca, and G. Strangi, Appl. Phys. Lett. **103**, 023107 (2013).
[29] M. A. K. Othman, C. Guclu, and F. Capolino, Opt. Express **21**, 7614 (2013).

[30] M. A. K. Othman, C. Guclu, and F. Capolino, SPIE J. Nanophoton. **7**, 073089 (2013).
[31] S. A. Mikhailov and K. Ziegler, Phys. Rev. Lett. **99**, 016803 (2007).
[32] M. Jablan, H. Buljan, and M. Soljačić, Opt. Express **19**, 11236 (2011).
[33] A. Yariv and P. Yeh, *Optical Waves in Crystals* (Wiley, New York, 1983).
[34] O. Kidwai, S. V. Zhukovsky, and J. E. Sipe, Phys. Rev. A **85**, 053842 (2012).
[35] X. Ni, S. Ishii, M. D. Thoreson, V. M. Shalaev, S. Han, S. Lee, and A. V. Kildishev, Opt. Express **19**, 25242 (2011).
[36] S. V. Zhukovsky, A. A. Orlov, V. E. Babicheva, A. V. Lavrinenko, and J. E. Sipe, Phys. Rev. A **90**, 013801 (2014).
[37] W. Yan, M. Wubs, and N. A. Mortensen, Phys. Rev. B **86**, 205429 (2012).
[38] R. M. Corless, G. H. Gonnet, D. E. G. Hare, D. J. Jeffrey, and D. E. Knuth, Adv. Comput. Math. **5**, 329 (1996).
[39] O. Kidwai, S. V. Zhukovsky, and J. E. Sipe, Opt. Lett. **36**, 2530 (2011).
[40] Yu. V. Bludov, A. Ferreira, N. M. R. Peres, and M. I. Vasilevskiy, Int. J. Mod. Phys. B **27**, 1341001 (2013).
[41] Yu. V. Bludov, N. M. R. Peres, and M. I. Vasilevskiy, J. Opt. **15**, 114004 (2013).
[42] Z. Xu, C. Chen, S. Qing, Yang Wu, B. Wang, J. Teng, C. Zhang, and Q. Bao, Proc. SPIE **8923**, 89230C (2013).
[43] G. Hanson, J. Appl. Phys. **103**, 064302 (2008).
[44] D. S. L. Abergel, V. Apalkov, J. Berashevich, K. Ziegler, and T. Chakraborty, Adv. Phys. **59**, 261 (2010).
[45] A. Andryieuski and A. V. Lavrinenko, Opt. Express **21**, 9144 (2013).
[46] P. Tassin, T. Koschny, and C. Soukoulis, Science **341**, 620 (2013).
[47] H. Yan, T. Low, W. Zhu, Y. Wu, M. Freitag, X. Li, F. Guinea, P. Avouris, and F. Xia, Nat. Photon. **7**, 394 (2013).
[48] Y. Hao, M. S. Bharathi, L. Wang, Y. Liu, H. Chen, S. Nie, X. Wang, H. Chou, C. Tan, B. Fallahazad, H. Ramanarayan, C. W. Magnuson, E. Tutuc, B. I. Yakobson, K. F. McCarty, Y.-W. Zhang, P. Kim, J. Hone, L. Colombo, and R. S. Ruoff, Science **342**, 720 (2013).
[49] L. Wang, I. Meric, P. Y. Huang, Q. Gao, Y. Gao, H. Tran, T. Taniguchi, K. Watanabe, L. M. Campos, D. A. Muller, J. Guo, P. Kim, J. Hone, K. L. Shepard, and C. R. Dean, Science **342**, 614 (2013).